Supporting Information:

The Effect of Second Coordination Sphere Interactions on the Magnetic Anisotropy of Transition Metals

Sofie S. Leiszner,[a] Mauro Perfetti,[b] Emil Damgaard-Møller,[a] Yu-Sheng Chen,[c] and Bo B. Iversen*[a]

[a]Center for Integrated Materials Research, Department of Chemistry and iNANO, Aarhus University, Langelandsgade 140, DK-8000 Aarhus C, Denmark.

[b]Department of Chemistry "U. Schiff", University of Florence, via della Lastruccia 3-13, 50019 Sesto Fiorentino, Italy.

[c]ChemMatCARS, The University of Chicago, Lemont, IL 60439, USA.

Corresponding author:

*Email: bo@chem.au.dk

Table of Contents

Section 1. Crystallographic Information, Multipole Modelling and Structural Results

Table S1. Selected crystallographic details from the Single Crystal X-ray Diffraction experiment on **1**, also including details on the modelling of the data.

	$CoCl_2(SC(NH_2)_2)_4$ (**1**)
Empirical formula	$C_4 H_{16} Cl_2 Co N_8 S_4$
Formular weight (g/mol)	434.32
Crystal size (μm)	60
Crystal system	Tetragonal
Space group	$P4_2/n$
Wavelength	0.30996 Å
Radiation type	Synchrotron radiation
Temperature (K)	20(2)
a (Å)	13.4486(1)
b (Å)	13.4486(1)
c (Å)	9.0022(1)
V (Å^3)	1628.18(2)
Z	4
F(000)	884
ρ (g/cm^3)	1.772
μ (mm^{-1})	0.196
T_{min}, T_{max}	0.8881, 0.9403
$\sin(\theta)/\lambda_{max}$,(Å^{-1})	1.6661
$N_{measured}$	628033
$N_{discarded}$	10438
N_{unique}	31522
Average redundancy	19.41
Completeness (%)	99.9
R_{int}	0.0922
$R_w(F)$, $R_w(F^2)$	0.0136, 0.0268
Weighting scheme	$1/\sigma(F^2)^2$
$R(F)$, $R(F^2)$	0.0154, 0.0188
GOF	0.9746
ρ_{min}, ρ_{max} (e/Å^3)	0.32, -0.34
No. of reflections used in the refinement	11413
No. of parameters refined	294
No. of reflections used in the refinement / parameters refined	38.82

Table S2. Applied symmetries used in the refinement of the multipole model on **1**. All listed symmetries are pseudo-symmetries that are applied to reduce the number of refined multipole population parameters, except for Co. Co occupies a special position of inversion

symmetry and therefore possesses a strict symmetry. In the refinement, only the listed population parameters of the spherical harmonic functions (rightmost column) are refined in XD02016.[1] The spherical harmonic functions given in parentheses were not refined, since inclusion of these high order spherical harmonic functions did not significantly improve the model.

Atoms	Symmetry	Spherical harmonic functions ($lm\pm$)
Co	$\bar{1}$	20, 21±, 22±, 40, 41±, 42±, 43±, 44±
Cl, S(1), S(2)	$m \perp x$	11±, 20, 21-, 22+, 30, 31-, 32+, 33-, 40, 41-, 42+, 43-, 44+
N(1), N(2), N(3), N(4), C(1), C(2)	mm2	10, 20, 22+, 30, 32+ (40, 42+, 44+)
All H-atoms	$\infty \parallel z$	10, 20 (30, 40)

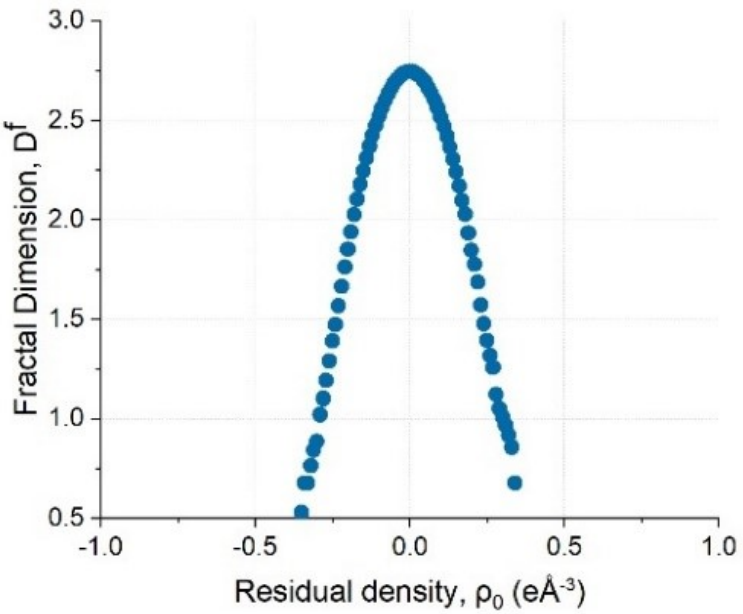

Fig. S1. Plot of the fractal dimension versus the residual density for the experimental multipole model of **1**.

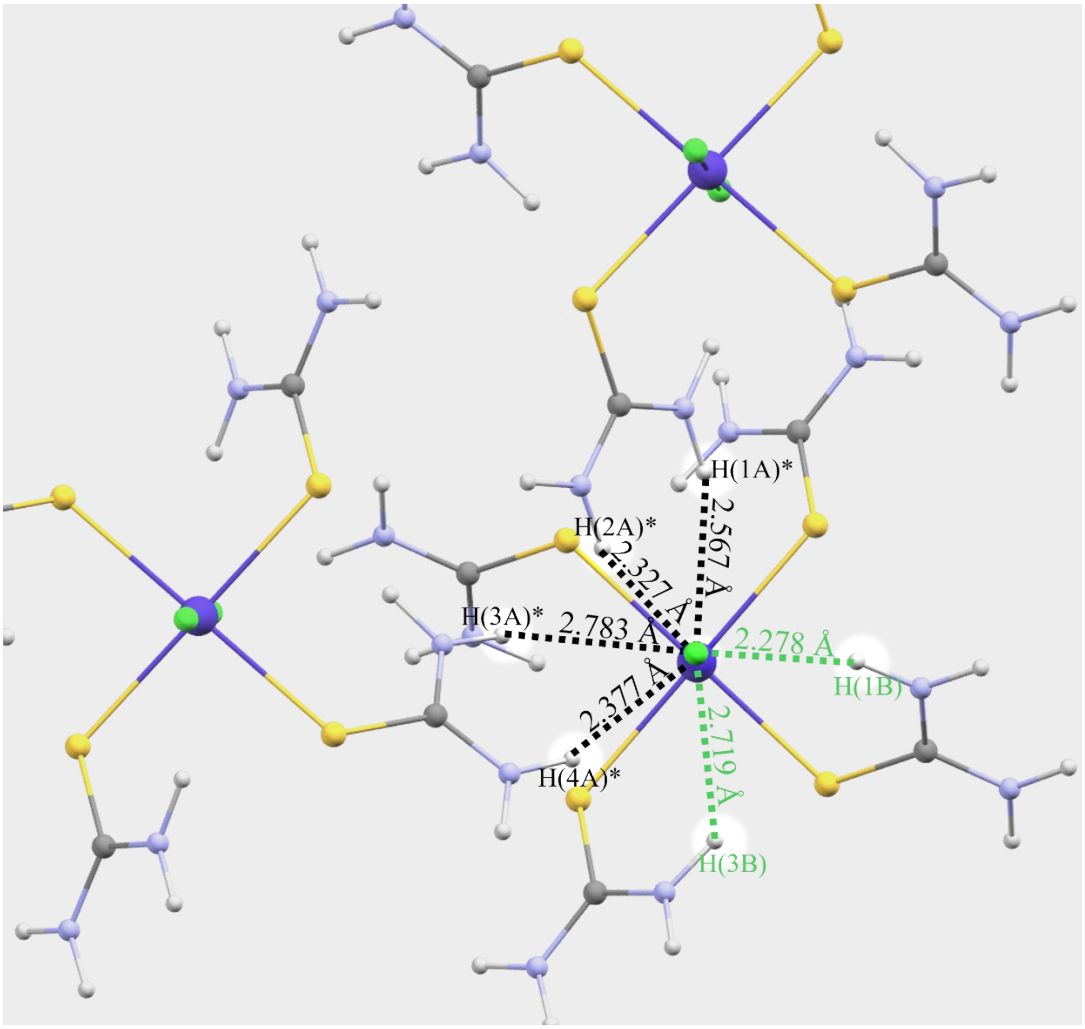

Fig. S2. Single Crystal X-ray Diffraction structure of **1** viewed along the Co-Cl axis. The two molecules in the crystal structure with hydrogen atoms close to Cl are shown. The distance from Cl to H for the two intramolecular (green) and the four intermolecular H-Cl distances (black) are given in Å. Atoms marked with a star (*) are from another molecule of **1** in the crystal structure (intermolecular interactions). H(1A)* and H(2A)* are generated by performing the symmetry operation $(y,\bar{x},\bar{z})$ along with the translation (-1, 1/2, 3/2), and H(3A)* and H(4A)* are generated by performing the symmetry operation $(\bar{y},x,\bar{z})$ and translation (1/2, 1/2, 2). The distances including uncertainties are listed in Table S3. Atom colors: Co (dark blue), Cl (green), S (yellow), N(light blue), C (grey) and H (white).

Table S3. Relevant bond lengths and angles in the crystal structure of **1** based on the multipole model from the Single-Crystal X-ray Diffraction (XRD columns) and the non-polarized Neutron Diffraction model by Tripathi *et al*[2] (ND columns).

Bond lengths (Å)			Bond angles (°)		
	XRD	*ND*		*XRD*	*ND*
Co − Cl	2.4657(1)	2.461(2)	S(1) − Co − Cl	92.270(2)	92.27(7)
Co − S(1)	2.50638(4)	2.501(3)	S(2) − Co − Cl	95.481(3)	95.44(7)
Co − S(2)	2.54953(4)	2.548(3)	S(1)' − Co − Cl	87.730(2)	87.73(7)
			S(2)' − Co − Cl	84.519(3)	84.56(7)
			S(1) − Co − S(2)	87.725(1)	87.76(9)
			S(1) − Co − S(2)'	92.28(1)	92.24(9)

Table S4. Distances to nearby H-atoms in the crystal based on the Single-Crystal X-ray diffraction structure (XRD column) and on the neutron diffraction structure (ND column).[2] Distances and angles involving intermolecular interactions are marked with a star (*). Uncertainties on the Co-H bond lengths for XRD are not given since the Co position cannot be refined as Co occupies a special position of inversion symmetry.

Distance (Å)			Bond angle (°)		
	XRD	*ND*		*XRD*	*ND*
Cl − H(1B)	2.2782(1)	2.277(4)	Co−Cl−H(1B)	82.073(3)	82.1
Cl − H(3B)	2.71905(9)	2.704(4)	Co−Cl−H(3B)	73.222(3)	73.1
Cl − H(1A)*	2.56704(9)	2.566(4)	Co−Cl−H(1A)*	88.769(3)	88.4
Cl − H(2A)*	2.3269(1)	2.324(5)	Co−Cl−H(2A)*	123.558(4)	123.8
Cl − H(3A)*	2.7832(1)	2.784(4)	Co−Cl−H(3A)*	80.542(3)	80.5
Cl − H(4A)*	2.3769(1)	2.376(4)	Co−Cl−H(4A)*	104.492(4)	104.0
Co − H(1B)	3.1178	3.115			
Co − H(3B)	3.0988	3.082			
Co − H(1A)*	3.5210	3.506			
Co − H(2A)*	4.2234	4.222			
Co − H(3A)*	3.4016	3.399			
Co − H(4A)*	3.8292	3.813			

Section 2. Cantilever Torque Magnetometry

Table S5. The orientation of the rotation axis and the magnetic field for the three orientations of the single crystal of **1** used for measuring CTM. The axes are given in the a'b'c* basis system of the crystal, in this case corresponding to a' = a / |a|, b' = b / |b|, c* = a' × b'.

Rotation number	Rotation axis	Magnetic Field axis
1	(-0.4866, 0.4866, -0.7256)	(0.707, 0.7070, 0)
2	(-0.707, -0.7070, 0)	(-0.4866, 0.4866, -0.7256)
3	(-0.5130, 0.5130, 0.6881)	(-0.4866, 0.4866, -0.7256)

Table S6: Fitted parameters in Cantilever Torque Magnetometry. The first three parameters (ρ, ξ and ψ) are the Euler angles in the extrinsic *x*-convention. The last three are the fitted eigenvalues of the effective $\bar{g}'$ matrix.

ρ	ξ	ψ	g_1	g_2	g_3
19.0	43.5	354.6	2.67	3.79	6.94

Table S7: The orientation of the three magnetic axes based on CTM.

Method	*x*	*y*	*z*
Easy axis	-0.06516	0.6855	0.7251
Intermediate axis	0.2589	0.7134	-0.6512
Hard axis	0.9637	-0.1453	0.2239

Table S8: The orientation of the easy axes for the different methods.

Method	*x*	*y*	*z*
Cantilever Torque Magnetometry (CTM)	-0.06516	0.6855	0.7251
CASSCF-NEVPT2	-0.07633	0.4208	0.9039
Polarized Neutron Diffraction (PND)	0.05982	0.5632	0.8242

Table S9: The angle given in degrees between the easy axes from different methods and the Co-Cl bond.

Method	CASSCF-NEVPT2	PND	Co-Cl bond
CTM	18.4°	11.5°	39.7°
CASSCF-NEVPT2		12.2°	21.6°
PND			30.8°

Section 3. Quantum Theory of Atoms In Molecules: Multipole Modelling Results

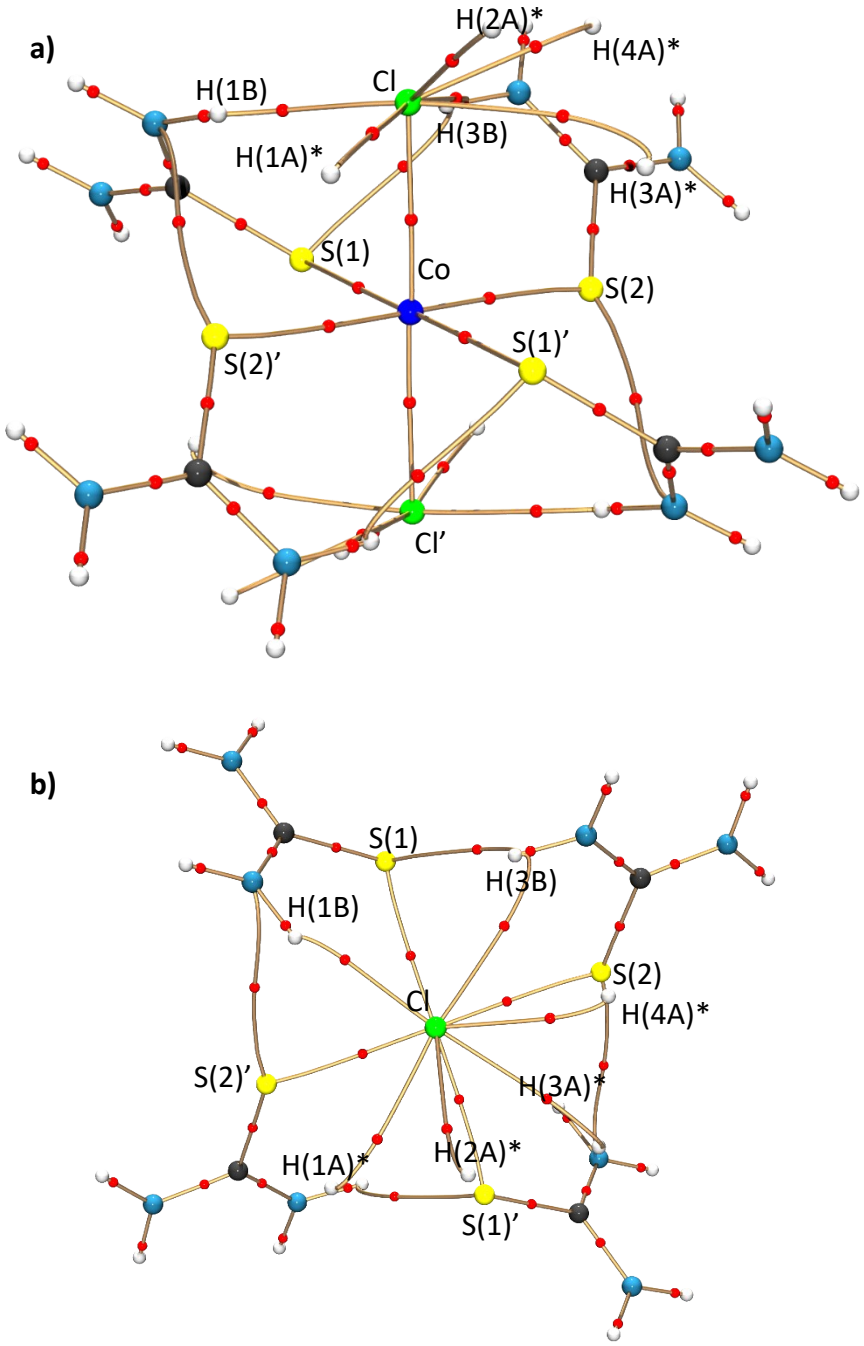

Fig. S3. Critical points and bond paths in the charge density seen from the side (a) and along the Co-Cl bond (b). Cl' and its critical points and bond paths are omitted from the plot in b) for clarity. Bond critical points are marked with red spheres and bond paths are represented by golden cylinders. H-atoms from other molecules in the crystal are marked with a star (*) and atoms from the other asymmetric units are marked with an apostrophe ('). Aom colors: Co (dark blue), N (light blue), S (yellow), Cl (green), C (dark grey) and H (white).

Table S10. Topological properties of the Cl-H and Co-ligand BCPs in **1**. The Hessian eigenvalues ($^{\lambda_i, i=1,2,3}$), ellipticity (ε), kinetic energy (G_b), the ratio of the kinetic energy and the electron density (G_b/ρ_{BCP}), the potential energy (V_b) and the total energy (E_b) at the BCP are listed for selected Cl-H BCPs. BCPs involving H-atoms from other molecules (intermolecular) are marked with a star (*).

Bond	λ_1 (e/Å^5)	λ_2 (e/Å^5)	λ_3 (e/Å^5)	ε	G_b (e/Å^3)	G_b/ρ_{BCP}	V_b (e/Å^3)	E_b (e/Å^3)
Cl-H(1B)	**-0.45**	**-0.40**	**2.68**	**0.12**	**0.11**	**0.94**	**-0.09**	**0.02**
Cl-H(3B)	-0.19	-0.17	1.14	0.15	0.04	0.72	-0.03	0.01
Cl-H(1A)*	-0.20	-0.20	1.36	0.02	0.05	0.83	-0.04	0.01
Cl-H(2A)*	**-0.33**	**-0.31**	**2.27**	**0.06**	**0.09**	**0.97**	**-0.07**	**0.02**
Cl-H(3A)*	-0.13	-0.10	0.89	0.37	0.04	0.75	-0.03	0.01
Cl-H(4A)*	**-0.31**	**-0.29**	**2.06**	**0.08**	**0.08**	**0.92**	**-0.06**	**0.02**
Co-Cl	-0.97	-0.84	6.16	0.15	0.28	1.13	-0.26	0.02
Co-S(1)	-1.08	-0.94	5.80	0.15	0.28	0.96	-0.29	-0.01
Co-S(2)	-0.86	-0.82	5.19	0.05	0.25	0.96	-0.25	0.00

Table S11. Characteristics of the Cl-H and Co-ligand bond critical points in **1**. d_1 and d_2 are the distance from the critical point to the first and second atom, respectively. ρ_{BCP} is the electron density at the bond critical point and $\nabla^2\rho_{BCP}$ is the Laplacian of the electron density in the bond critical point. BCP's involving H-atoms from other molecules (intermolecular) are marked with a star (*).

Bond	d_1 (Å)	d_2 (Å)	ρ_{BCP} (e/Å^3)	$\nabla^2\rho_{BCP}$ (e/Å^5)
Cl-H(1B)	**1.5452**	**0.7463**	**0.115**	**1.836**
Cl-H(3B)	1.7117	1.0679	0.061	0.779
Cl-H(1A)*	1.6903	0.9231	0.064	0.967
Cl-H(2A)*	**1.5652**	**0.7841**	**0.095**	**1.640**
Cl-H(3A)*	1.7701	1.0797	0.047	0.655
Cl-H(4A)*	**1.5849**	**0.8211**	**0.090**	**1.458**
Co-Cl	1.1036	1.3625	0.25	4.35
Co-S(1)	1.0937	1.4142	0.29	3.78
Co-S(2)	1.1064	1.4448	0.26	3.51

Static Deformation Density	Negative Laplacian
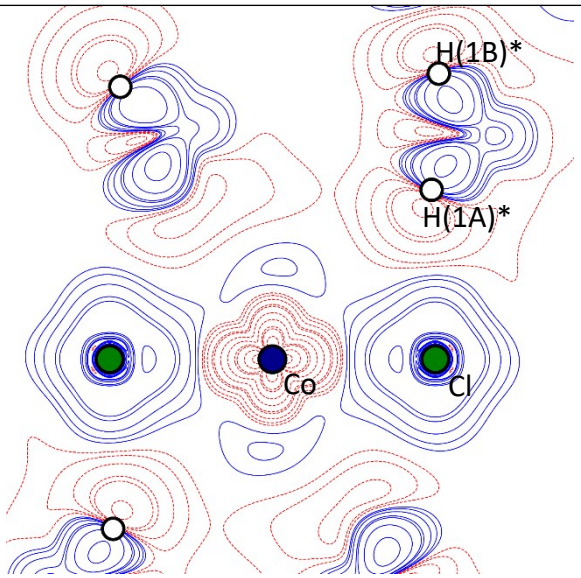	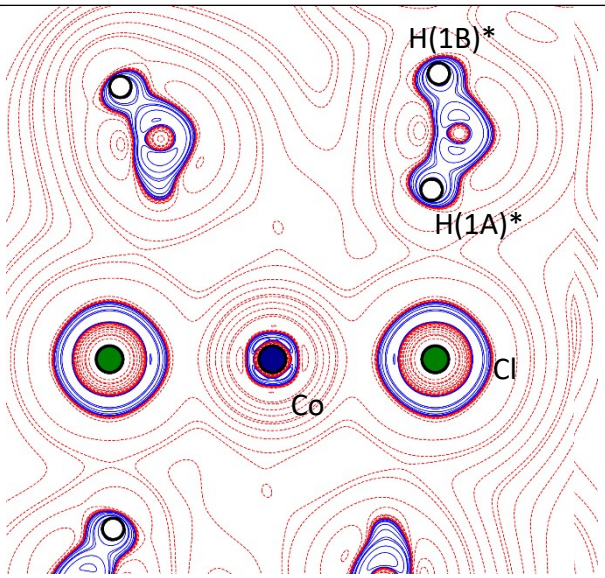
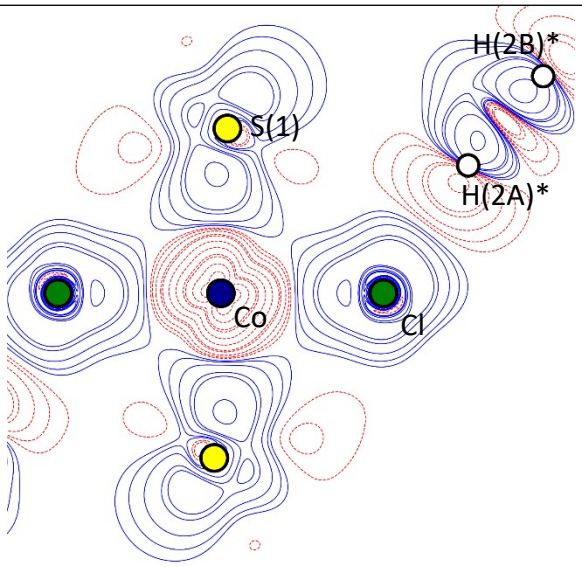	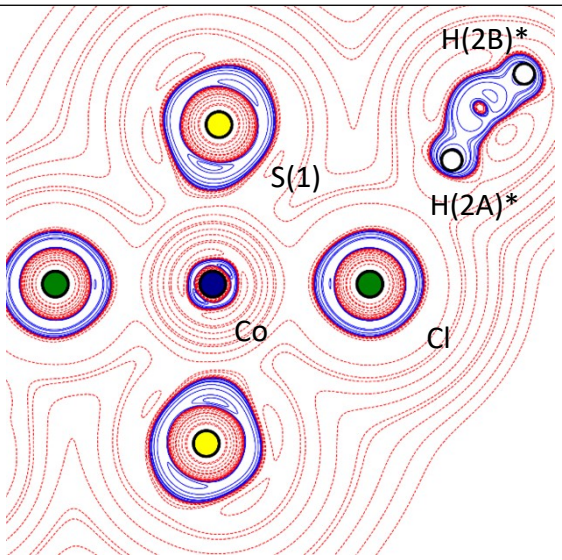
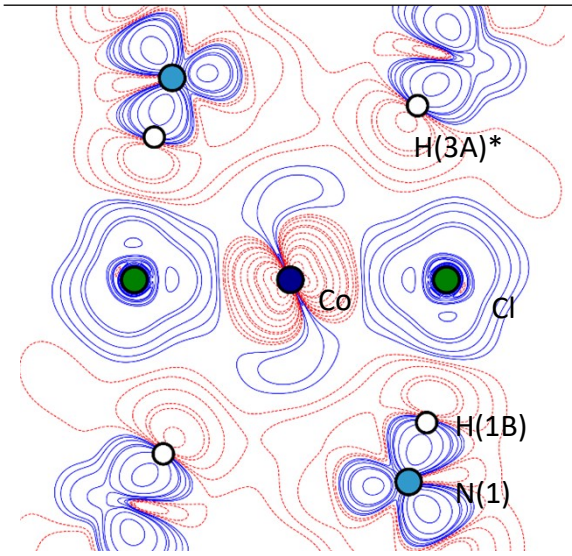	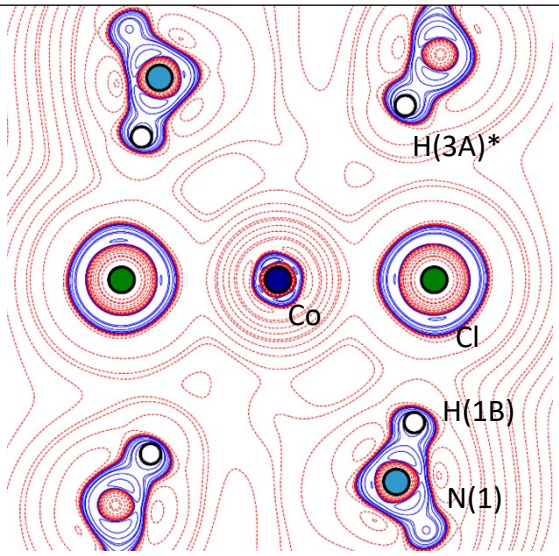

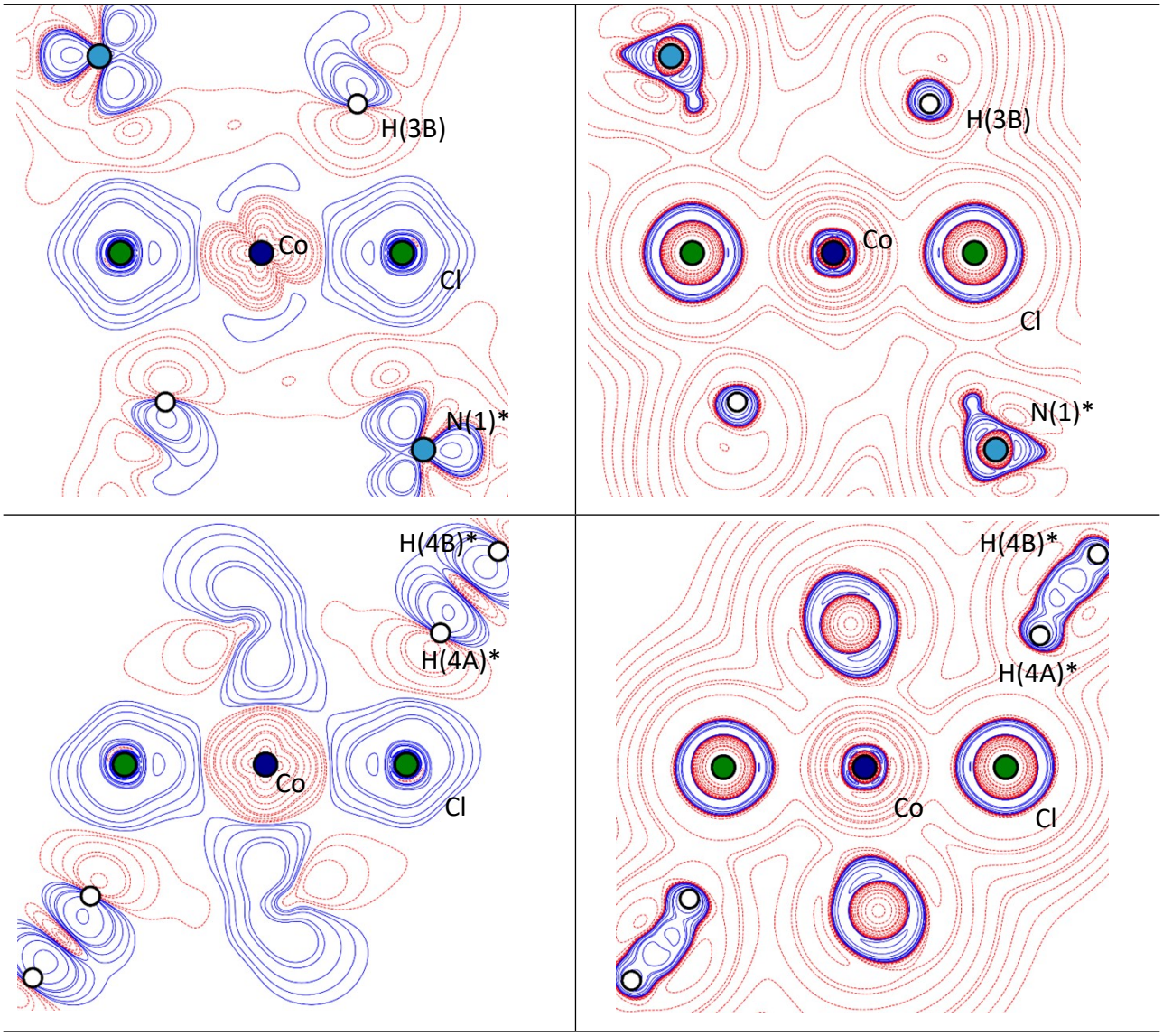

Fig. S4. 2D plot of the static deformation density (left column) and the negative Laplacian, $-\nabla^2\rho(r)$. Dashed red lines indicate negative contours and solid blue lines indicate positive contours. The rows correspond to the following planes: Co-Cl-H(1A)*, Co-Cl-H(2A)*, Co-Cl-H(3A)*, Co-Cl-H(3B), Co-Cl-H(4A)*. The contour lines for the static deformation density are drawn from −2.0 e/Å^3 to 2.0 e/Å^3 in linear steps of 0.05 e/Å^3. Negative Laplacian contour lines are drawn at: $a \cdot 10^n$ e/Å^5, with a = 1, 2, 4, 8 and n = -2, -1, 0, 1, 2, 3, 4.

Remarks on the negative Laplacian:

Analogous to the electron density, critical points can also be found in the negative Laplacian $L(\boldsymbol{r}) \equiv -\nabla^2\rho(\boldsymbol{r})$. Visualizing these critical points in Valence Shell Charge Concentration (VSCC), will show the distortion of the valence density around Co(II) caused by chemical bonding.[3, 4]

The atomic graph showing the critical points in the VSCC for Co is shown below, including the (3, +3) critical points in the Valence Shell Charge Depletion (VSCD). An atomic graph for an octahedral complex typically shows six (3, −3) charge concentrations, twelve (3, −1) saddle points, and six pairs of (3, +1) saddle points and (3, +3) charge depletions along the metal-ligand bonds.[3] The atomic graph for **1** does in fact show the expected amount of (3, −3) and (3, −1) CPs, but has two extra pairs of (3, +1) saddle points and (3, +3) charge depletions. These two pairs form an axis that show approximate 3-fold symmetry in the Laplacian CPs. This axis is directed towards the face of the octahedron formed by Cl, S(2) and S(1)'. The presence of additional (3, +1) and (3, +3) CPs is typical for tetrahedral complexes, making it a rather unusual topology of the Laplacian for **1**.

The other pairs of (3, +1) and (3, +3) CPs are approximately directed towards the metal-ligand bonds. The pair closets to the Co-Cl axis forms an angle of 10.6° with the Co-Cl axis and an angle of 26.8° with respect to the easy axis from CTM.

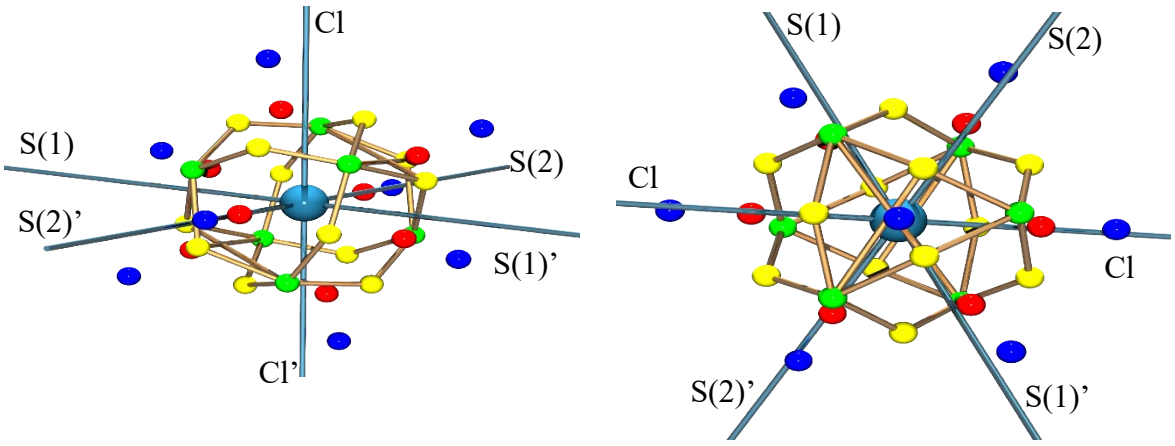

Fig. S5. Atomic graph for Co showing the critical points for the negative Laplacian, $L(r) \equiv -\nabla^2\rho(r)$, in the VSCC and (3,+3) critical points in the VSCD. (3, −3), (3, −1), (3, +1) and (3, +3) critical points are marked with green, yellow, red, and blue, respectively. The light blue cylinders are bonds, and the atom labels indicate which atom a given bond is directed towards. Two different perspectives: a) sideview of the octahedron and b) view along pseudo-3-fold axis.

Section 4. Theoretical Calculations: CASSCF-NEVPT2

All theoretical calculations have been performed in ORCA 4.1[5], and all analysis of wavefunctions have been performed in AIMAll.[6]

Subsection 4a. Comparison of experimental and theoretical electron density

Negative Laplacian: Experimental Electron Density	Negative Laplacian: Electron density from CASSCF wavefunction
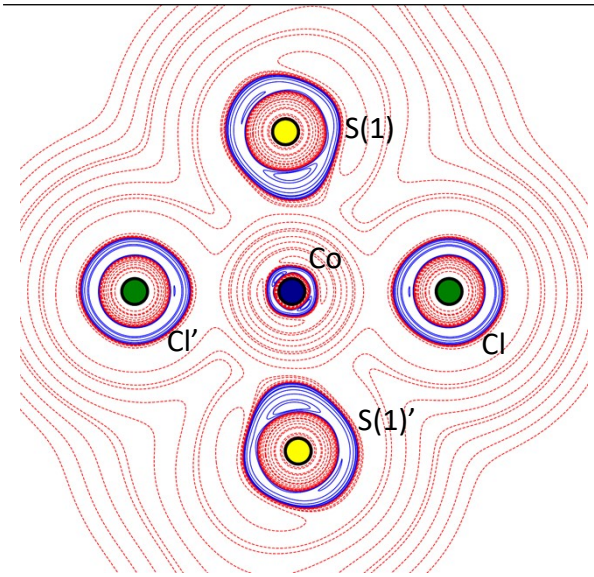	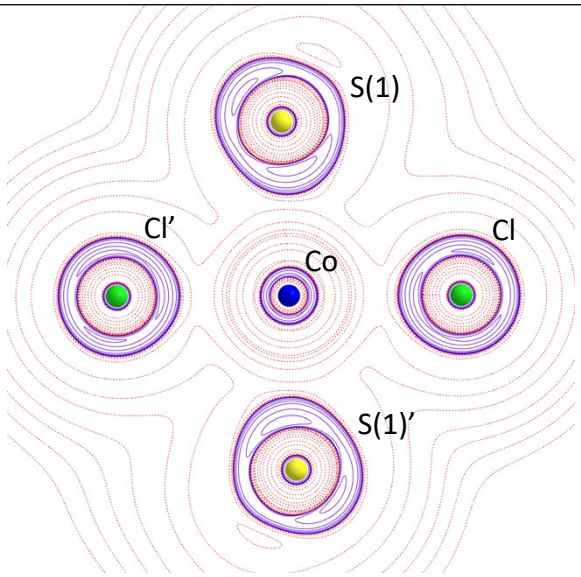
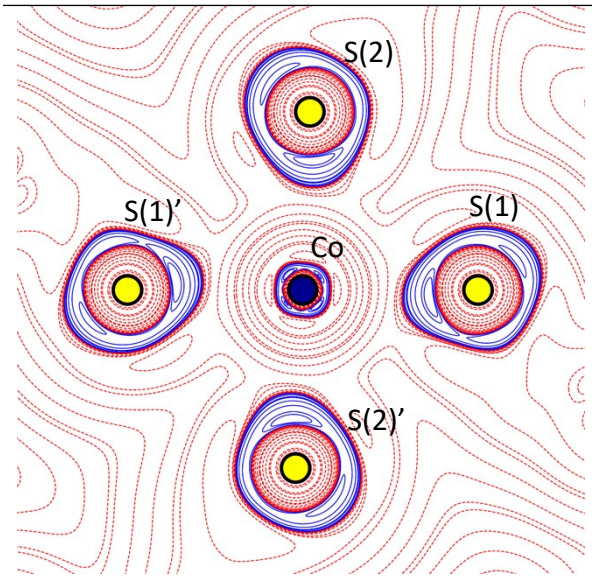	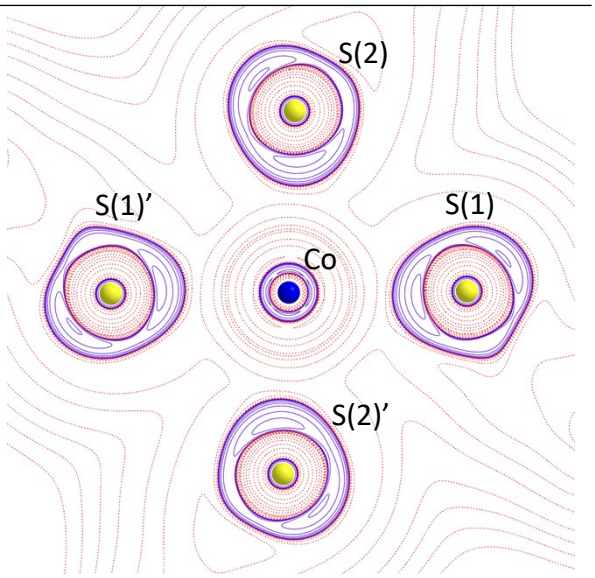

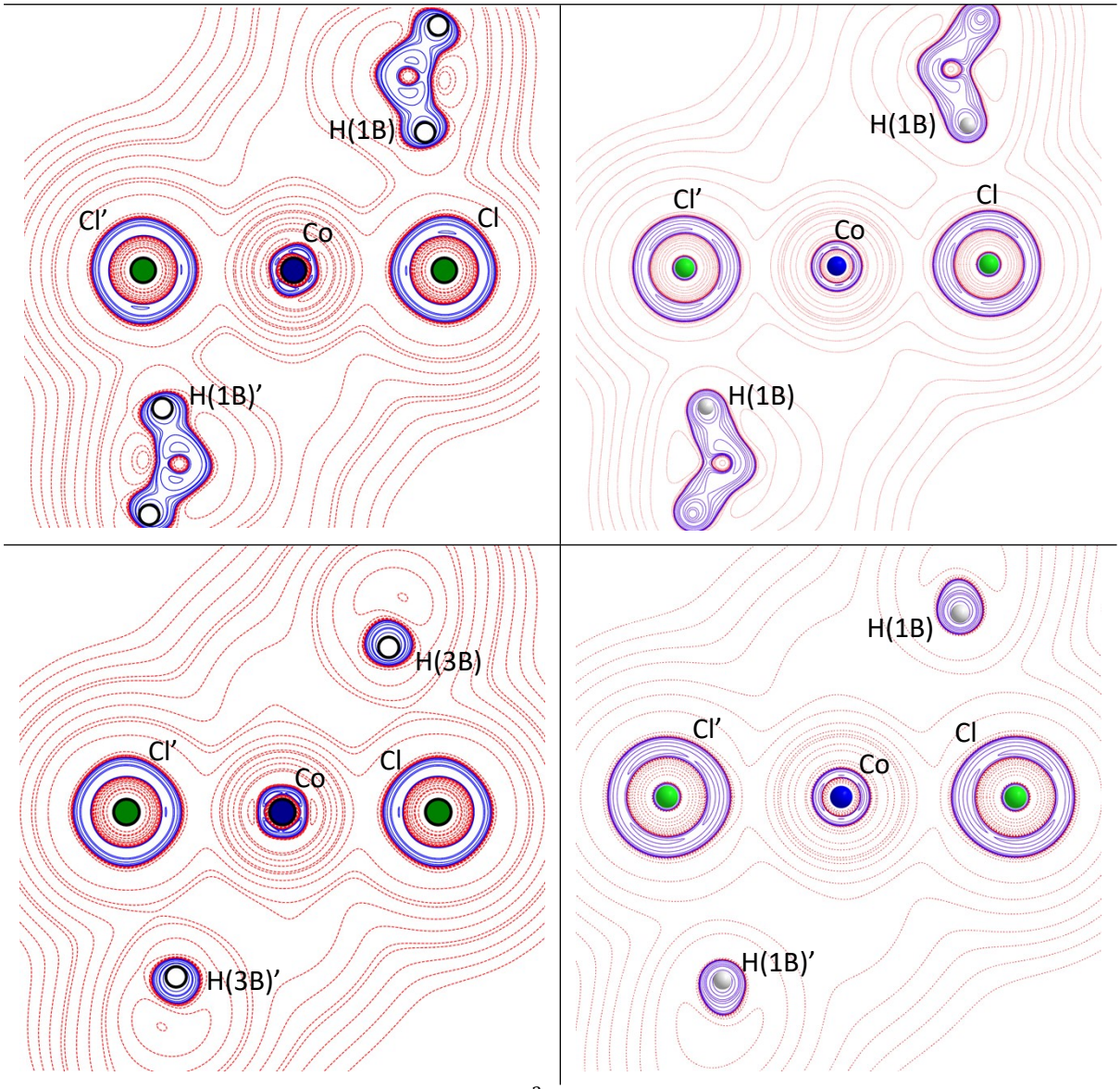

Fig. S6. 2D plot of the negative Laplacian, $-\nabla^2\rho(r)$. Dashed red lines indicate negative contours and solid blue lines indicate positive contours. The rows correspond to the following planes: S-Co-Cl, S-Co-S, Co-Cl-H(1B), Co-Cl-H(3B). The plots in the left column are calculated based on the experimental electron density model using XD2016[1], and the negative Laplacian contours are drawn at $a \cdot 10^n$ e/Å^5, with a = 1, 2, 4, 8 and n = -2, -1, 0, 1, 2, 3, 4. The right column are calculated based on the CASSCF wavefunction using AimAll[6], and contours are drawn at the following values in units of e/a_0^5 (a_0 being the Bohr radius): 0.0, ±0.001, ±0.002, ±0.004, ±0.008, ±0.02, ±0.04, ±0.08, ±0.2, ±0.4, ±0.6, ±0.8, ±1.4, ±2, ±4, ±8, ±20, ±42, ±80, ±200, ±400 and ±800.

Table S12. Comparison of the characteristics of the Bond Critical Points (BCPs) from the experimental multipole model of the charge density (given in non-italic, top rows) and from the theoretical wavefunction (given in italic, lower rows). ρ_{BCP} is the electron density at the BCP and $\nabla^2\rho_{BCP}$ is the Laplacian of the electron density at the BCP. In addition, the Hessian eigenvalues ($\lambda_i, i = 1,2,3$), the ellipticity (ε), the kinetic energy density (G), the potential energy density (V) and the total energy (E) at the BCP are given. Overall, the values from the experimental multipole model agree well with those from the CASSCF wavefunction, which justifies the reliability of the theoretical results. The Laplacian values at the S-C BCPs differ significantly between the two models. While both the experimental and theoretical electron density are flat in this the central region of the C-S bond, the Laplacian, which amplifies the local variations in the electron density, show significant variations in this region. The BCP is displaced towards the S-atom in the theoretical model leading to the higher Laplacian values for the theoretical wavefunction.

BCP	ρ_{BCP} (e/Å^3)	$\nabla^2\rho_{BCP}$ (e/Å^5)	λ_1 (e/Å^5)	λ_2 (e/Å^5)	λ_3 (e/Å^5)	ε	G (e/Å^3)	V (e/Å^3)	E (e/Å^3)
Co - Cl	0.25	4.35	-0.97	-0.84	6.16	0.15	0.28	-0.26	0.02
	0.316	*4.22*	*-1.12*	*-1.12*	*6.46*	*0.00*	*0.34*	*-0.38*	*-0.04*
Co - S(1)	0.29	3.78	-1.08	-0.94	5.80	0.15	0.28	-0.29	-0.01
	0.316	*3.67*	*-1.15*	*-1.08*	*5.90*	*0.07*	*0.31*	*-0.35*	*-0.05*
Co - S(2)	0.26	3.51	-0.86	-0.82	5.19	0.05	0.25	-0.25	0.00
	0.289	*3.36*	*-1.02*	*-0.97*	*5.34*	*0.06*	*0.27*	*-0.31*	*-0.04*
Cl - H(1B)	0.11	1.84	-0.45	-0.40	2.68	0.12	0.11	-0.09	0.02
	0.139	*1.64*	*-0.55*	*-0.54*	*2.73*	*0.02*	*0.10*	*-0.09*	*0.01*
Cl - H(3B)	0.06	0.78	-0.19	-0.17	1.14	0.15	0.04	-0.03	0.01
	0.0628	*0.84*	*-0.18*	*-0.14*	*1.16*	*0.25*	*0.05*	*-0.03*	*0.01*
S(1) - C(1)	1.44	-5.84	-7.82	-6.84	8.82	0.14	1.20	-2.81	-1.61
	1.36	*0.17*	*-5.51*	*-4.32*	*9.99*	*0.28*	*1.56*	*-3.10*	*-1.54*
S(2) - C(2)	1.44	-5.79	-7.78	-6.86	8.85	0.13	1.21	-2.82	-1.61
	1.38	*0.66*	*-5.74*	*-4.36*	*10.77*	*0.32*	*1.62*	*-3.20*	*-1.58*
S(1) - H(3B)	0.10	1.05	-0.36	-0.29	1.70	0.23	0.07	-0.06	0.01
	0.098	1.16	-0.33	-0.28	1.78	0.17	0.07	-0.06	0.01

N(1) - C(1)	2.45	-30.42	-20.50	-17.80	7.88	0.15	2.17	-6.47	-4.30
	2.45	*-29.50*	*-22.41*	*-21.13*	*14.04*	*0.06*	*2.29*	*-6.64*	*-4.35*
N(2) - C(1)	2.41	-27.89	-19.99	-17.10	9.20	0.17	2.19	-6.33	-4.14
	2.41	*-27.07*	*-21.87*	*-21.43*	*16.23*	*0.02*	*2.39*	*-6.67*	*-4.28*
N(3) - C(2)	2.40	-28.14	-19.35	-17.14	8.36	0.13	2.14	-6.25	-4.11
	2.43	*-29.53*	*-22.17*	*-20.82*	*13.47*	*0.06*	*2.23*	*-6.53*	*-4.30*
N(4) - C(2)	2.39	-27.57	-19.32	-16.82	8.57	0.15	2.15	-6.22	-4.08
	2.40	*-26.89*	*-21.77*	*-21.28*	*16.16*	*0.02*	*2.37*	*-6.63*	*-4.25*
N(4) - H(4B)	1.99	-31.53	-28.15	-26.66	23.28	0.06	1.05	-4.31	-3.26
	2.32	*-49.53*	*-34.09*	*-32.53*	*17.09*	*0.05*	*0.30*	*-4.07*	*-3.77*
N(1) - H(1A)	1.99	-31.56	-28.16	-26.62	23.22	0.06	1.05	-4.31	-3.26
	2.28	*-44.59*	*-31.86*	*-30.48*	*17.74*	*0.05*	*0.33*	*-3.78*	*-3.45*
N(1) - H(1B)	1.99	-31.47	-28.13	-26.59	23.26	0.06	1.06	-4.33	-3.26
	2.28	*-54.31*	*-36.04*	*-34.84*	*16.57*	*0.03*	*0.27*	*-4.34*	*-4.07*
N(2) - H(2A)	1.97	-30.92	-27.82	-26.27	23.17	0.06	1.06	-4.28	-3.22
	2.27	*-44.16*	*-31.69*	*-30.15*	*17.68*	*0.05*	*0.33*	*-3.74*	*-3.42*
N(2) - H(2B)	1.97	-30.82	-27.77	-26.22	23.17	0.06	1.06	-4.27	-3.21
	2.39	*-53.42*	*-36.10*	*-34.49*	*17.18*	*0.05*	*0.31*	*-4.36*	*-4.05*
N(3) - H(3A)	1.98	-31.06	-27.96	-26.35	23.25	0.06	1.06	-4.29	-3.23
	2.28	*-44.35*	*-31.76*	*-30.33*	*17.74*	*0.05*	*0.33*	*-3.77*	*-3.44*
N(3) - H(3B)	1.98	-30.76	-27.83	-26.20	23.27	0.06	1.07	-4.29	-3.22
	2.30	*-53.98*	*-35.90*	*-34.67*	*16.60*	*0.04*	*0.27*	*-4.32*	*-4.05*
N(4) - H(4A)	1.99	-31.49	-28.13	-26.64	23.28	0.06	1.05	-4.31	-3.26
	2.29	*-44.84*	*-32.08*	*-30.50*	*17.74*	*0.05*	*0.33*	*-3.80*	*-3.47*

Subsection 4b. Towards D_{4h} symmetry in the first coordination sphere

Table S13. For each of the structures modified towards D_{4h} symmetry in the first coordination sphere, the Cl-H(1B) distance in the structure is listed along the angle between the easy axis and Co-Cl bond and the *D*-value.

Description	$d_{Cl\text{-}H1B}$/ Å	Angle(g^{calc}_{zz}, Co-Cl) / °	*D* / cm^{-1}
$\mathbf{1}^{ND}$	2.277	21.52	-81.08
$d(Co\text{-}S)_{avg}$	2.294	21.67	-81.63
$d(Co\text{-}S)_{avg}$ and $\angle_{SCoS}$ = 90°	2.294	22.96	-94.78
$1^{ND}_{D_{4h}}$	2.382	21.97	-105.4

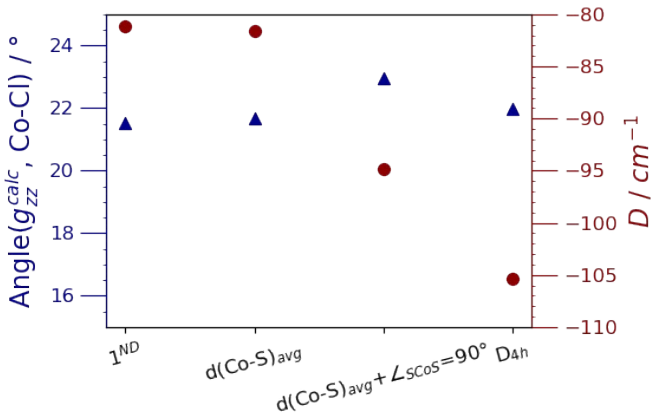

Fig. S7. The angle between the CASSCF easy axis and the Co–Cl bond (blue triangles) and the *D*-value (red circles) plotted for $\mathbf{1}^{ND}$ structures modified towards D_{4h} symmetry in the first coordination sphere.

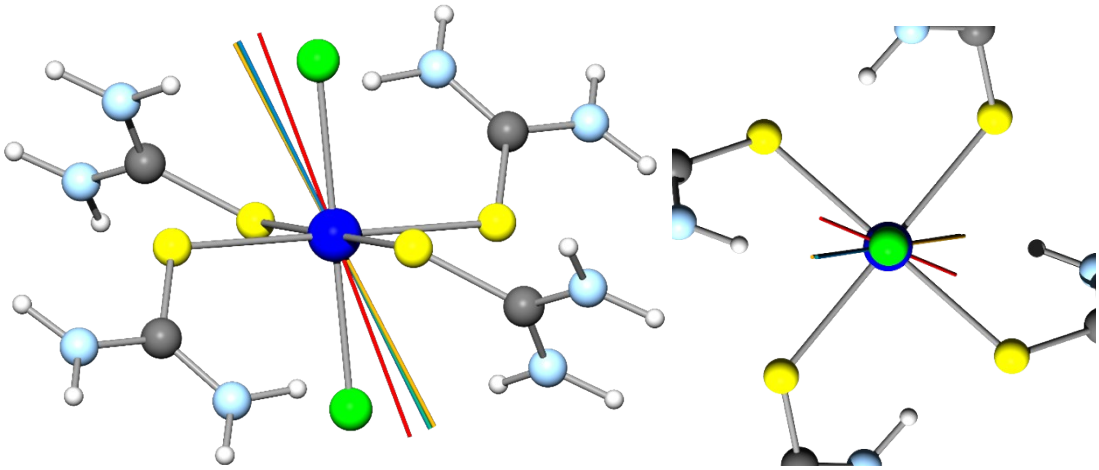

Fig. S8. The **1**ND structure[2] seen from the side (left) and along the Cl-Co bond (right) with the calculated easy axes for the towards first coordination sphere D_{4h} symmetry. Color code for the calculated easy axes: the **1**ND easy axis is orange, the easy axis for the structure with Co-S distances set to the average distance is green, the easy axis for the structure with average Co-S distances and S-Co-S angles of 90° is blue and the easy axis for the structure with perfect D_{4h} geometry in the 1st coordination sphere, referred to as ${}^{1}D_{4h}^{ND}$, is red.

Subsection 4c. C-N rotations on the 1^{ND} structure

Table S14. The rotation angle along C(1)-N(1), φ_1, the rotation angle around C(2)-N(3), φ_2, the Cl-H(1B) distance, $d_{Cl\text{-}H1B,}$ and the Cl-H(3B) distance, $d_{Cl\text{-}H3B}$, for each structure used to obtain the results in Figure 7-9 of the manuscript are listed. The modifications are performed on the $\mathbf{1}^{ND}$ structure. The angle between the calculated easy axis and the Co-Cl bond, Angle(g_{zz}^{calc}, Co-Cl), and the extracted *D*- and *E*-values are also listed for each structure.

φ_1 / rad.	Φ_2 / rad.	$d_{Cl\text{-}H1B}$/ Å	$d_{Cl\text{-}H3B}$/ Å	Angle(g_{zz}^{calc}, Co-Cl) / °	*D* / cm^{-1}	*E* / cm^{-1}
-π/32	0	2.267	2.704	21.64	-80.83	-18.68
0	0	2.277	2.704	21.52	-81.08	-18.51
π/32	0	2.298	2.704	21.27	-81.58	-18.33
2π/32	0	2.329	2.704	20.90	-82.29	-18.14
3π/32	0	2.371	2.704	20.44	-83.23	-17.99
4π/32	0	2.423	2.704	19.90	-84.35	-17.85
5π/32	0	2.482	2.704	19.30	-85.61	-17.77
6π/32	0	2.549	2.704	18.67	-86.92	-17.71
7π/32	0	2.622	2.704	18.04	-88.29	-17.68
8π/32	0	2.699	2.704	17.43	-89.47	-17.66
9π/32	0	2.780	2.704	16.85	-90.61	-17.66
10π/32	0	2.864	2.704	16.32	-91.57	-17.66
11π/32	0	2.949	2.704	15.86	-92.31	-17.66
12π/32	0	3.035	2.704	15.48	-92.80	-17.68
13π/32	0	3.121	2.704	15.19	-92.97	-17.70
14π/32	0	3.206	2.704	15.00	-92.78	-17.74
14.5π/32	0	3.249	2.704	14.94	-92.54	-17.77
14.5π/32	π/32	3.249	2.773	14.65	-94.50	-17.73
14.5π/32	2π/32	3.249	2.846	14.60	-94.50	-17.77
14.5π/32	3π/32	3.249	2.925	14.40	-96.62	-17.88
14.5π/32	4π/32	3.249	3.007	14.20	-98.83	-18.04
14.5π/32	5π/32	3.249	3.092	14.00	-101.0	-18.23
14.5π/32	6π/32	3.249	3.178	13.80	-103.1	-18.44
14.5π/32	7π/32	3.249	3.265	13.70	-104.9	-18.66
14.5π/32	8π/32	3.249	3.351	13.60	-106.3	-18.89
14.5π/32	9π/32	3.249	3.437	13.46	-108.0	-19.11

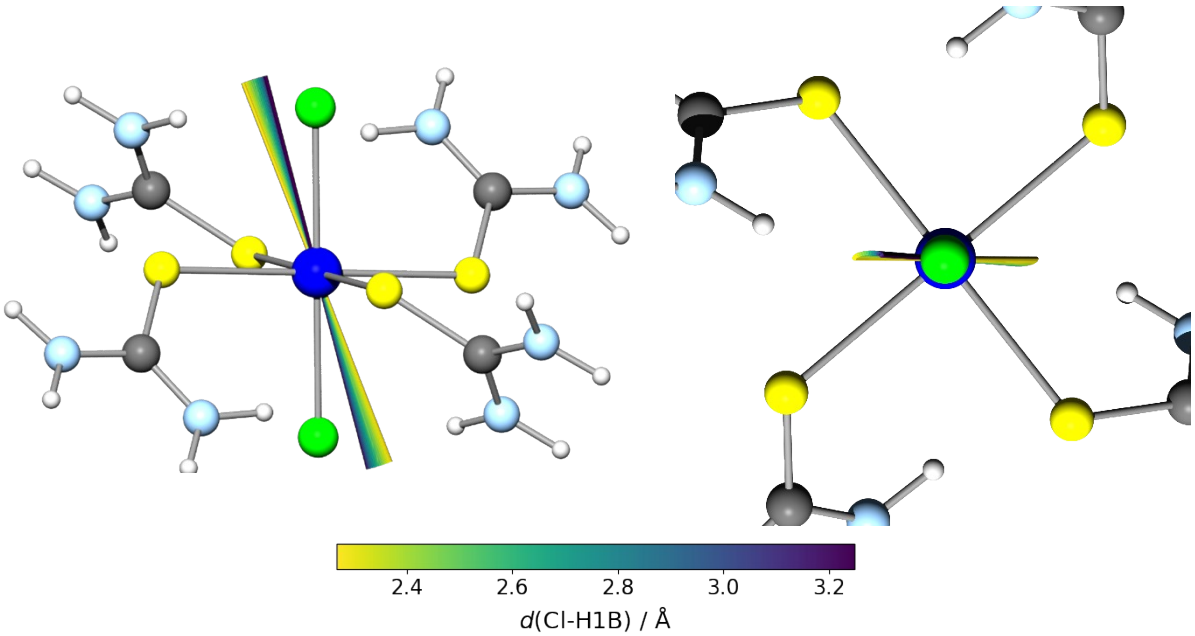

Fig. S9. The **1**ND structure seen from the side (left) and along the Cl-Co bond (right) with the calculated easy axes after the C(1)-N(1) rotations (only φ_1 rotations). A color gradient is added to visualize the easy axes' dependence on Cl-H(1B) distance, *d*(Cl-H1B).

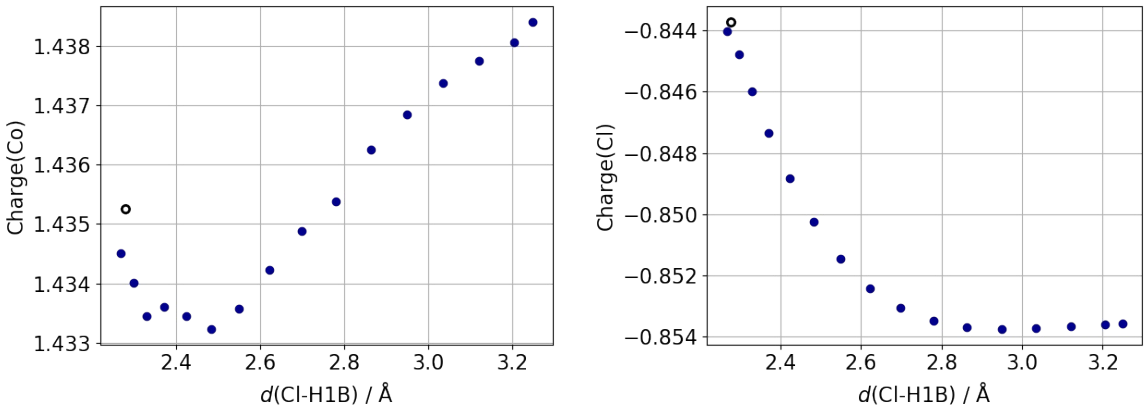

Fig. S10. Charge of Co (left) and Cl(right) based on integration in AIMAll versus the Cl-H(1B) distance for each modified structure from the C(1)-N(1) rotations (only φ_1 rotations). The result of the CASSCF calculation on **1**ND structure is shown as an open circle in black.

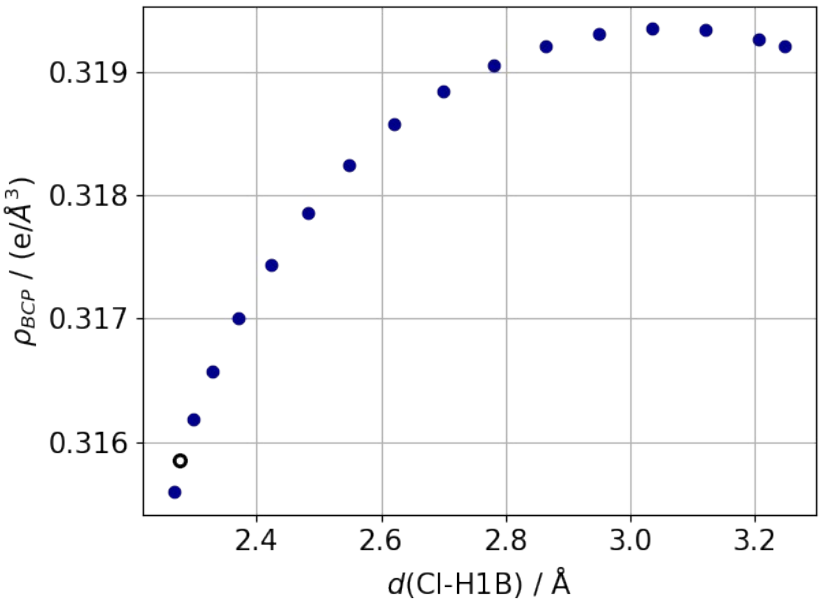

Fig. S11. Electron density in the Co-Cl Bond Critical Point (BCP) versus the Cl-H(1B) distance for each modified structure from the C(1)-N(1) rotations (only φ_1 rotations). The result of the CASSCF calculation on **1**ND structure is shown as an open circle in black.

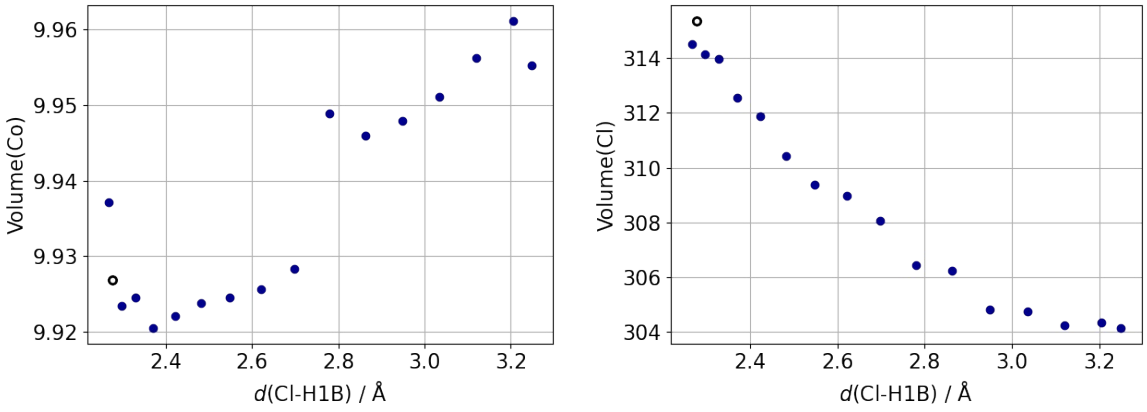

Fig. S12. Volume of Co (left) and Cl(right) based on integration in AIMAll[6] versus the Cl-H(1B) distance for each modified structure from the C(1)-N(1) rotations (only φ_1 rotations). The result of the CASSCF calculation on **1**ND structure is shown as an open circle in black.

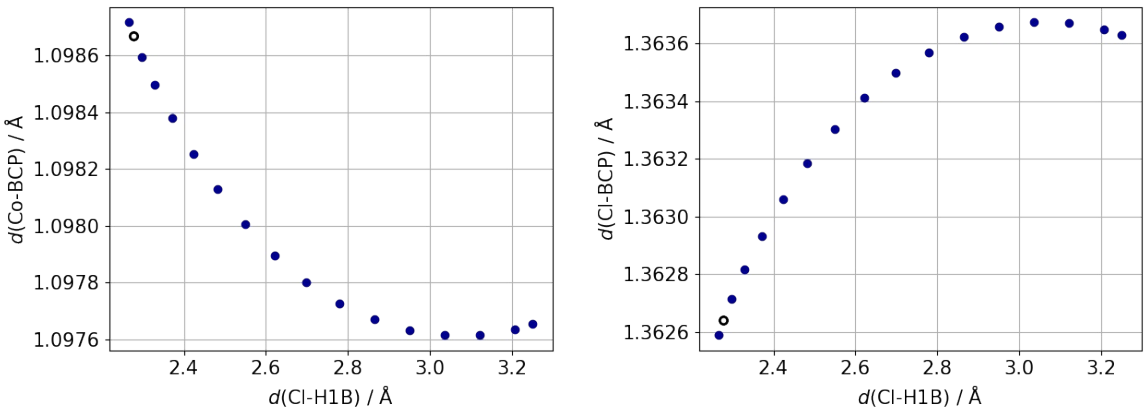

Fig. S13. Distance from Co to the Co-Cl BCP (left) and distance from Cl to the Co-Cl BCP (right) versus the Cl-H(1B) distance for each modified structure from the C(1)-N(1) rotations (only φ_1 rotations). The result of the CASSCF calculation on **1**ND structure is shown as an open circle in black.

Subsection 4d. C-N rotations on the $1_{D_{4h}}^{ND}$ structure

Table S15. The rotation angle along C(1)-N(1), φ_1, the rotation angle around C(2)-N(3), φ_2, the Cl-H(1B) distance, $d_{\text{Cl-H1B}}$, and the Cl-H(3B) distance, $d_{\text{Cl-H3B}}$, for each structure used to obtain the results in Figure 7-9 of the manuscript are listed. The modifications are performed on the modified **1**ND structure with D_{4h} symmetry in the 1st coordination sphere, referred to as $1_{D_{4h}}^{ND}$. The angle between the calculated easy axis and the Co-Cl bond, Angle(g_{zz}^{calc}, Co-Cl), and the extracted *D*- and *E*-values are also listed for each structure.

φ_1 / rad.	φ_2 / rad.	$d_{\text{Cl-H1B}}$/ Å	$d_{\text{Cl-H3B}}$/ Å	Angle(g_{zz}^{calc}, Co-Cl) / °	*D* / cm^{-1}	*E* / cm^{-1}
-2π/32	0	2.363	2.467	21.96	-103.3	22.85
-π/32	0	2.367	2.467	22.03	-104.3	22.70
0	0	2.382	2.467	21.97	-105.4	22.51
π/32	0	2.409	2.467	21.78	-106.7	22.31
2π/32	0	2.446	2.467	21.48	-108.1	22.13
3π/32	0	2.493	2.467	21.08	-109.5	21.97
4π/32	0	2.548	2.467	20.59	-111.0	21.86
5π/32	0	2.611	2.467	20.04	-112.4	21.79
6π/32	0	2.681	2.467	19.46	-113.8	21.75
7π/32	0	2.756	2.467	18.85	-114.9	21.73
8π/32	0	2.836	2.467	18.26	-115.9	21.73
9π/32	0	2.919	2.467	17.69	-116.7	21.73
10π/32	0	3.004	2.467	17.17	-117.1	21.73
11π/32	0	3.090	2.467	16.70	-117.2	21.71
12π/32	0	3.176	2.467	16.30	-116.9	21.69
13π/32	0	3.262	2.467	15.97	-116.2	21.66
14π/32	0	3.347	2.467	15.72	-115.0	21.63
14π/32	π/32	3.347	2.538	15.23	-116.5	21.46
14π/32	2π/32	3.347	2.614	14.78	-118.3	21.38
14π/32	3π/32	3.347	2.695	14.40	-120.2	21.39
14π/32	4π/32	3.347	2.778	14.09	-122.2	21.48
14π/32	5π/32	3.347	2.864	13.83	-124.2	21.63
14π/32	6π/32	3.347	2.950	13.63	-126.1	21.85
14π/32	7π/32	3.347	3.037	13.47	-127.7	22.13
14π/32	8π/32	3.347	3.123	13.35	-129.1	22.42
14π/32	9π/32	3.347	3.208	13.27	-129.9	22.69

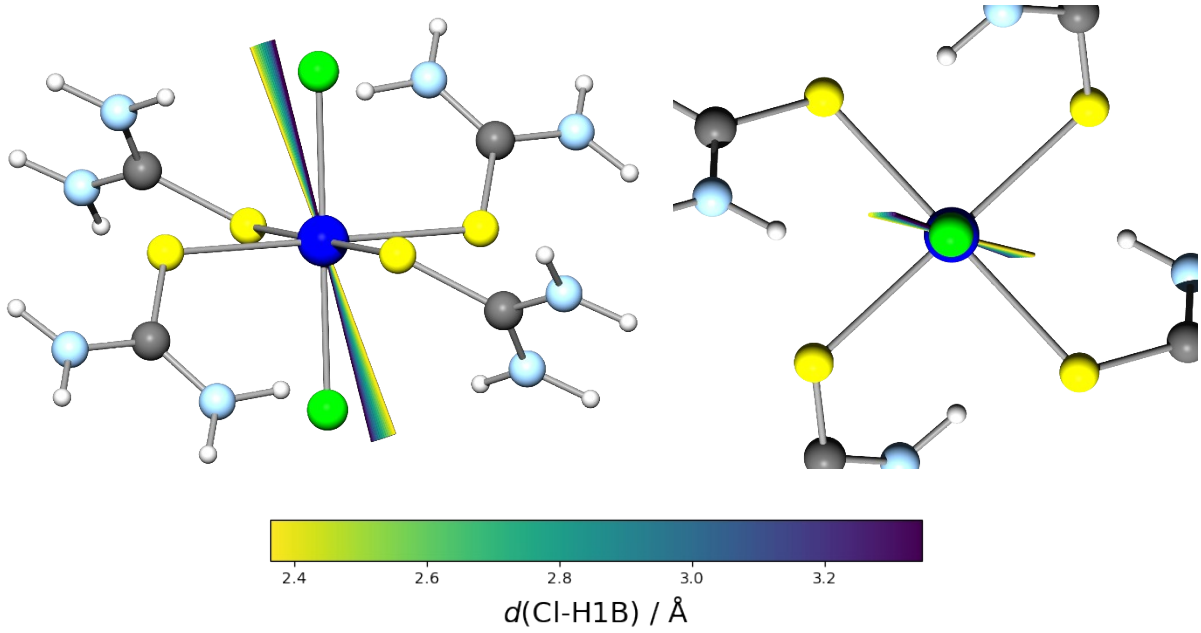

Fig. S14. The $\mathbf{1}^{ND}$ structure modified to have D_{4h} symmetry in the first coordination sphere, referred to as ${}^{1}_{D_{4h}}{}^{ND}$, seen from the side (left) and along the Cl-Co bond (right) with the calculated easy axes after the C(1)-N(1) rotations (only φ_1 rotations). A color gradient is added to visualize the easy axes' dependence on Cl-H(1B) distance, *d*(Cl-H1B).

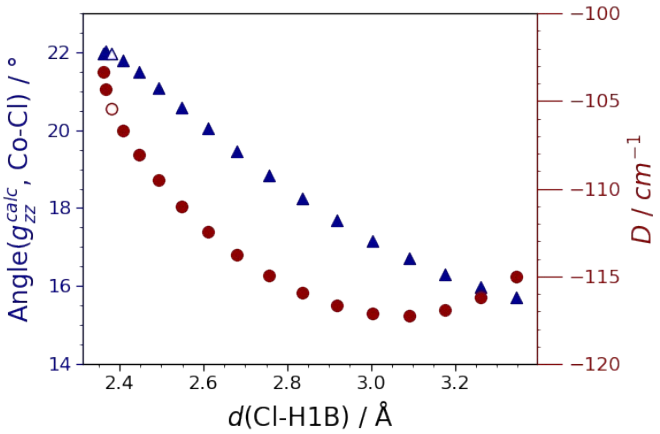

Fig. S15. The angle between the CASSCF easy axis and the Co−Cl bond (blue triangles) and the *D*-value (red circles) plotted as a function of the Cl−H(1B) distance for the *in silico* rotations

around C(1)-N(1) in the $1_{D_{4h}}^{ND}$ structure. The results from the CASSCF calculation on the $1_{D_{4h}}^{ND}$structure are shown as open symbols.

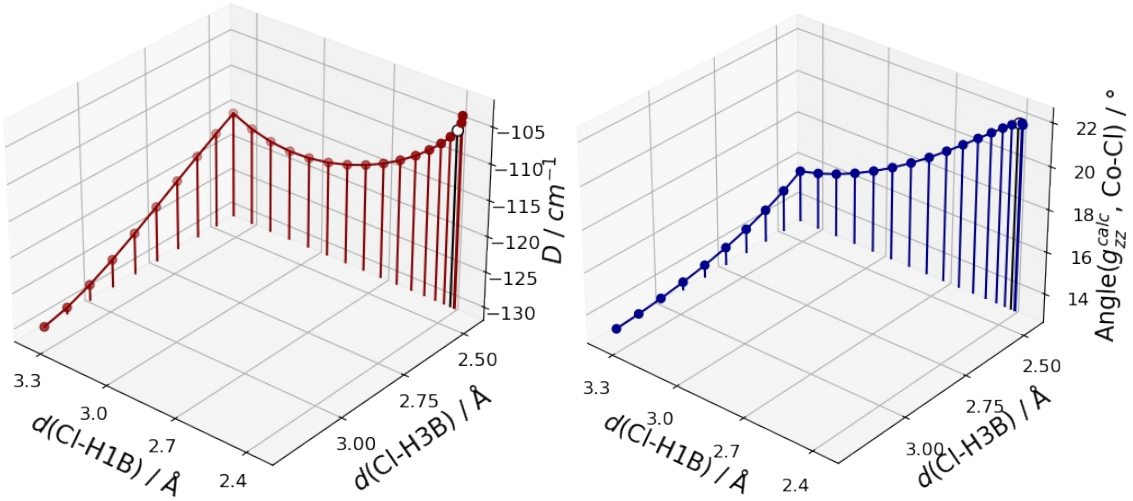

Fig. S16. The angle between the easy axis and the Co−Cl bond (left) and the *D*-value (right) plotted as a function of the Cl−H(1B) and Cl-H(3B) distance in the modified structures of $1_{D_{4h}}^{ND}$. This includes the rotations around C(1)-N(1), followed by rotations around C(2)-N(3). The results from the $1_{D_{4h}}^{ND}$ structure are shown as open circles in black.

Subsection 4e. C-S rotations on the 1^{ND} structure

Table S16. The rotation angle around the C=S bonds, φ_3, the minimum Cl-H distance for the given structure, d_{min}^{ClH}, for each of the structures used for CASSCF-NEVPT2 calculations are listed. All d_{min}^{ClH} are from Cl to H(1B), except those marked with [a] (distance to H(4B)) and are therefore not included in the results of the paper. The angle between the calculated easy axis and the Co-Cl bond, $\angle_{ea,CoCl}$, the angle between the calculated easy axis and the experimental easy axis from PND, $\angle_{PND,calc}$, and the extracted *D*- and *E*-values are also listed for each structure.

φ_3 / rad.	$d_{Cl\text{-}H1B}$/ Å	$\angle_{calc,CoCl}$ / °	$\angle_{calc,PND}$ / °	*D* / cm^{-1}	*E* / cm^{-1}
− 4π/32	2.346	23.99	10.40	-77.09	20.41
-3π/32	2.285	23.98	10.46	-76.59	20.07
-2π/32	2.252	23.52	10.77	-77.18	19.63
-π/32	2.249	22.69	11.37	-78.69	19.09
0	2.277	21.62	12.19	-81.08	18.51
π/32	2.333	20.45	13.14	-84.44	18.00
2π/32	2.417	19.25	14.10	-88.63	17.64
3π/32	2.523	18.03	15.03	-93.23	17.48
4π/32	2.649	16.81	15.92	-97.67	17.50
5π/32	2.790	15.62	16.78	-101.26	17.64
6π/32	2.943	14.50	17.61	-103.71	17.87
7π/32	3.106	13.51	18.37	-105.01	18.17
8π/32	3.275	12.67	19.05	-105.43	18.56
9π/32	3.447	11.99	19.64	-105.27	18.94
10π/32	3.621	11.50	20.09	-105.00	19.35
11π/32	3.795	11.23	20.35	-105.12	19.72
12π/32	3.968	11.20	20.40	-105.95	20.02
13π/32	4.137	11.37	20.26	-107.32	20.22

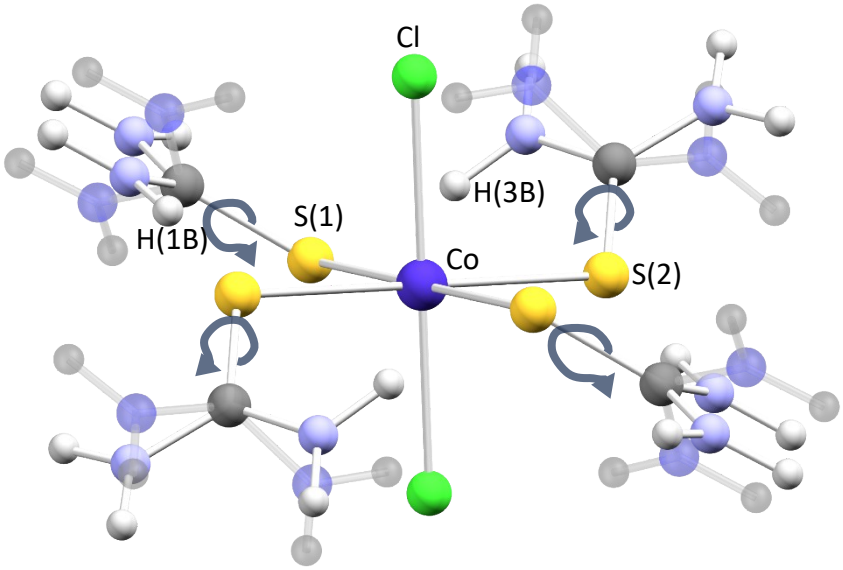

Fig. S17. The structure for a rotation of the thiourea ligands by $\varphi = \pi/4$ rad. The transparent structure is the experimental $\mathbf{1}^{ND}$ structure ($\varphi = 0$ rad.). The S(1)-C(1) and the S(2)-C(2) bonds are rotated clockwise, whereas the S(1)'-C(1)' and the S(2)'-C(2)' bonds are rotated anticlockwise to preserve the $\bar{1}$ symmetry at Co.

Table S17. The orientation of the easy axes for the different rotation around the S=C bonds.

φ_3 / rad.	*x*	*y*	*z*
− 4π/32	0.07501	-0.4587	-0.8854
-3π/32	0.07617	-0.4584	-0.8855
-2π/32	0.07615	-0.4511	-0.8892
-π/32	0.07603	-0.4379	-0.8958
0	0.07633	-0.4208	-0.9039
π/32	0.07656	-0.4018	-0.9125
2π/32	0.07552	-0.382	-0.9209
3π/32	0.07236	-0.3630	-0.9290
4π/32	0.06704	-0.3438	-0.9367
5π/32	0.06052	-0.3251	-0.9437
6π/32	0.05387	-0.3077	-0.9500
7π/32	0.04791	-0.2921	-0.9552
8π/32	0.04335	-0.2787	-0.9594
9π/32	0.04071	-0.2675	-0.9627
10π/32	0.03973	-0.2593	-0.9650
11π/32	0.03982	-0.2547	-0.9662
12π/32	0.04043	-0.2540	-0.9664
13π/32	0.04119	-0.2567	-0.9656

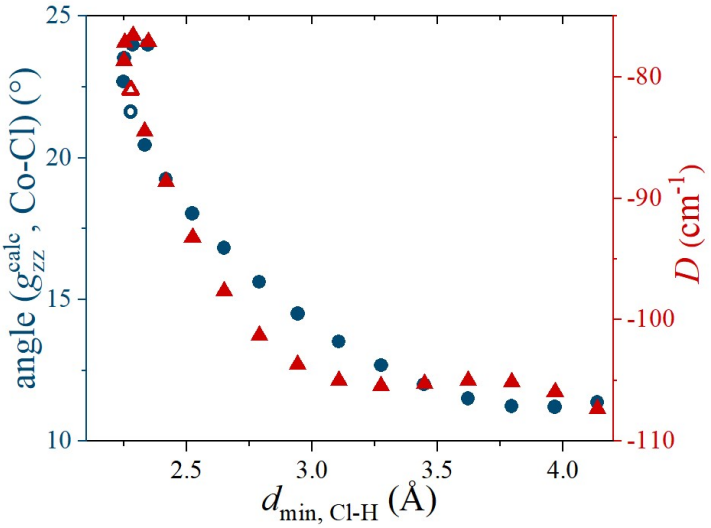

Fig. S18. The angle between the CASSCF easy axis and the Co−Cl bond (blue triangles) and the *D*-value (red circles) plotted as a function of the Cl−H(1B) distance for the *in silico* rotations around S=C in the **1**ND structure. The results from the CASSCF calculation on the $1_{D_{4h}}^{ND}$structure are shown as open symbols.

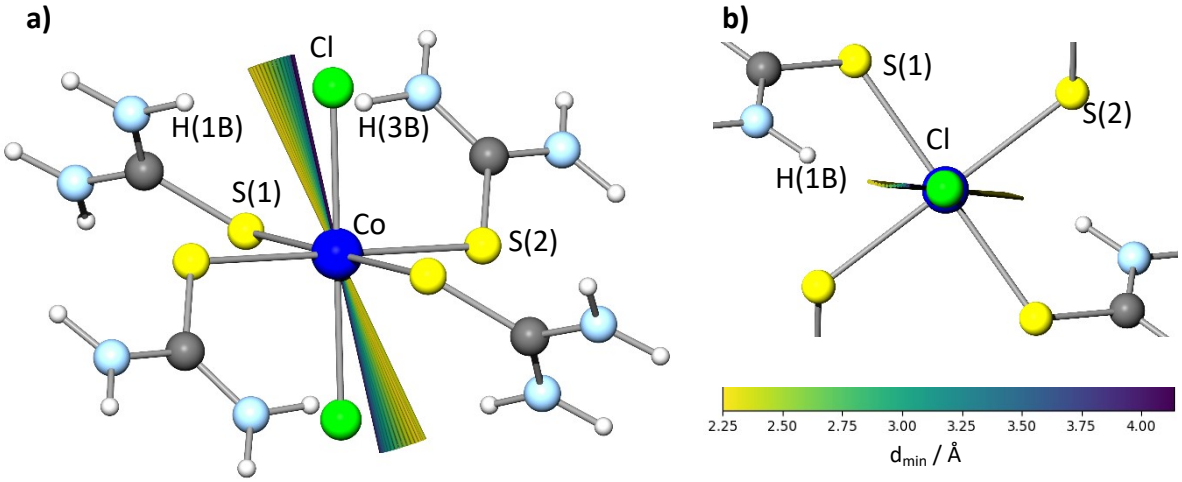

Fig. S19. The **1**ND structure seen from the side (a) and along the Cl-Co bond (b) with the calculated easy axes for the 18 rotations of the thiourea molecules. A color gradient is added to visualize the easy axes' dependence on d_{min}.

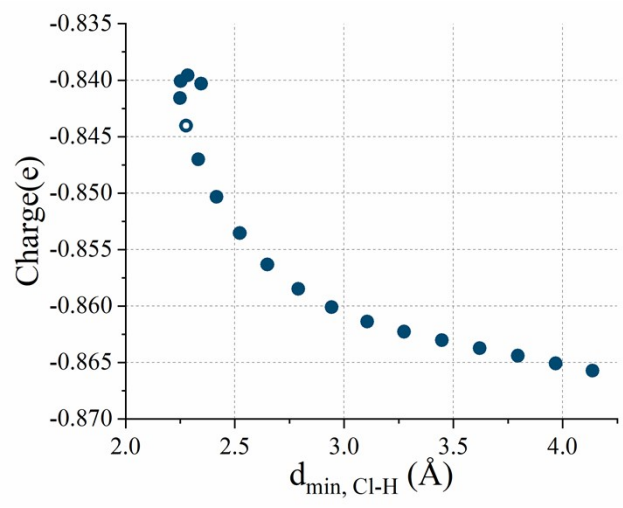

Fig. S20. The integrated charge on Cl vs. the minimum Cl-H distance in the permutated structures of **1**ND. The **1**ND structure is marked with an open circle.

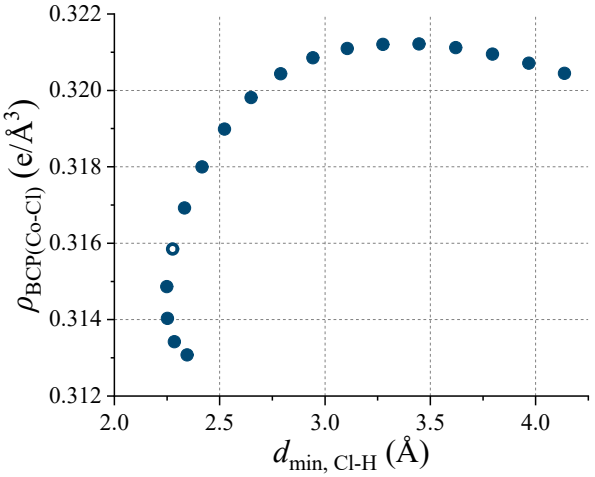

Fig. S21. Electron density in the Bond Critical Point between Co and Cl as function of the minimum Cl−H distance in each of the modified structures of **1**ND. The result of the CASSCF calculation on **1**ND structure is shown as an open circle.

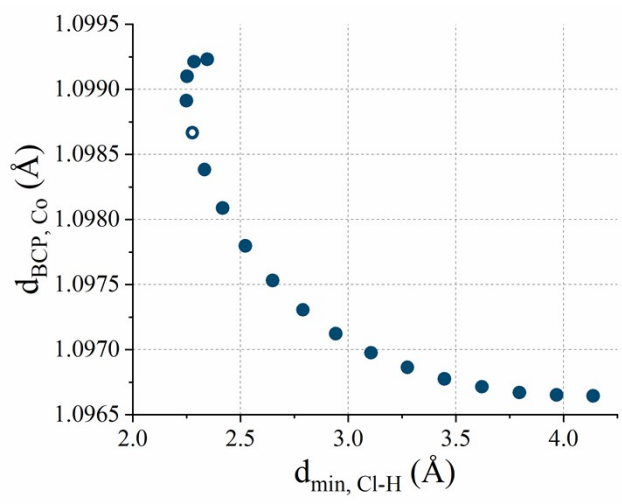

Fig. S22. The distance from Co to the BCP between Co and Cl vs. the minimum Cl-H distance in the permutated structures of **1**ND. The **1**ND structure is marked with an open circle.

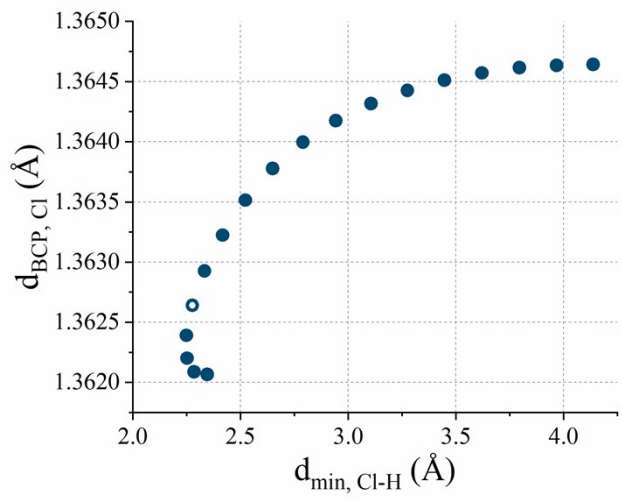

Fig. S23. The distance from Cl to the BCP between Co and Cl vs. the minimum Cl-H distance in the permutated structures of **1**ND. The **1**ND structure is marked with an open circle.

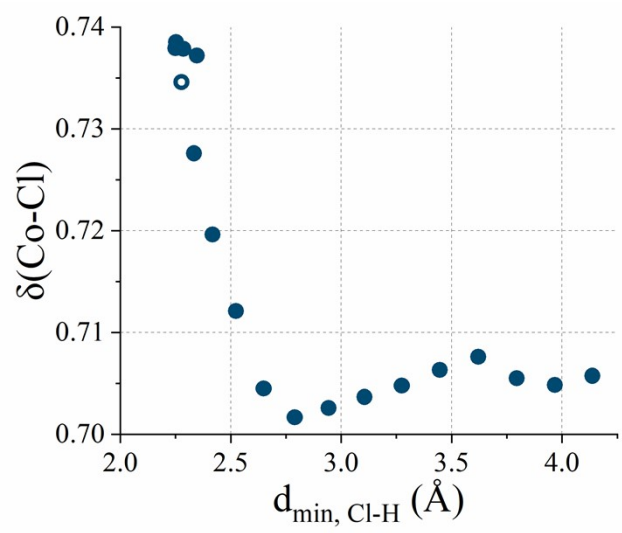

Fig. S24. The delocalization index between Co and Cl, δ(Co-Cl), vs. the minimum Cl-H distance in the permutated structures of **1**ND. The **1**ND structure is marked with an open circle.

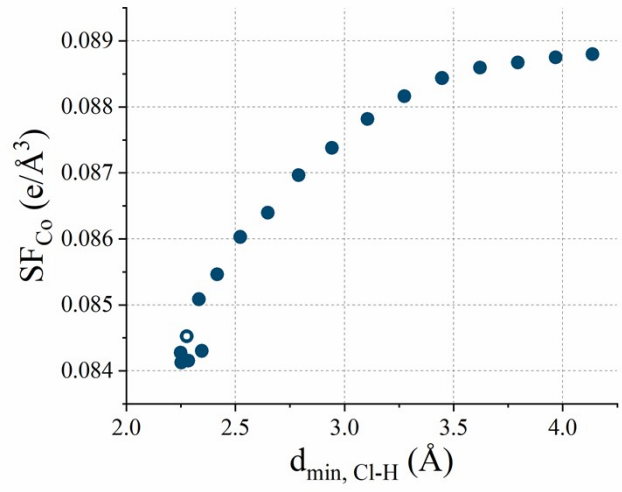

Fig. S25. The Source Function for Co calculated in the Bond Critical Point (BCP) between Co and Cl vs. the minimum Cl-H distance in the permutated structures of **1**ND. The **1**ND structure is marked with an open circle.

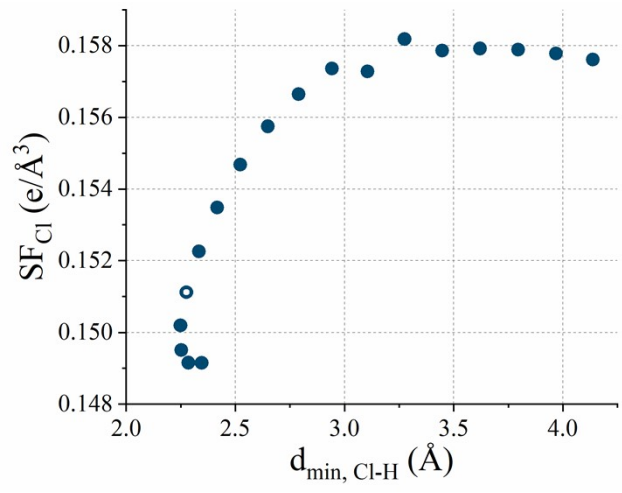

Fig. S26. The Source Function for Cl calculated in the Bond Critical Point (BCP) between Co and Cl vs. the minimum Cl-H distance in the permutated structures of **1**ND. The **1**ND structure is marked with an open circle.

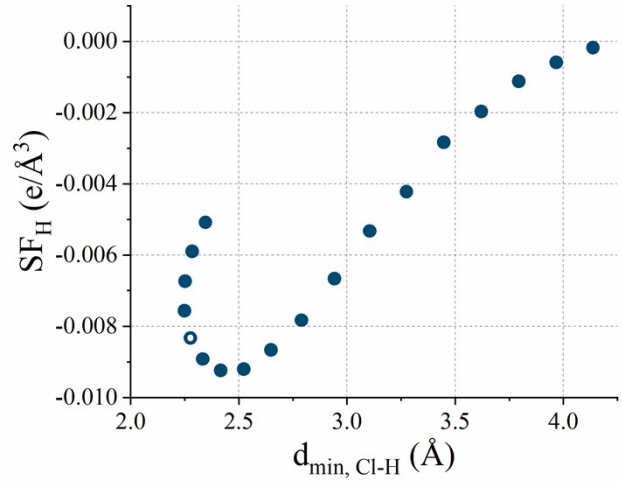

Fig. S27. The Source Function for H(1B) calculated in the Bond Critical Point (BCP) between Co and Cl vs. the minimum Cl-H distance in the permutated structures of **1**ND. The **1**ND structure is marked with an open circle.

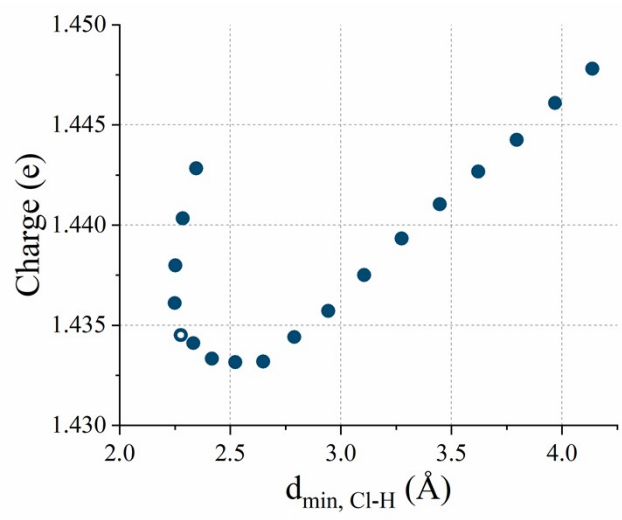

Fig. S28. The integrated charge on Co vs. the minimum Cl-H distance in the permutated structures of **1**ND. The **1**ND structure is marked with an open circle.

Section 5. References

1. P. M. A. Volkov, L. J. Farrugia, C. Gatti, P. Mallinson, T. Richter, T. Koritsanszky, XD2016 - A Computer Program Package for Multipole Renement, Topological Analysis of Charge Densities and Evaluation of Intermolecular Energies from Experimental and Theoretical Structure Factors, 2016.
2. S. Tripathi, S. Vaidya, N. Ahmed, E. Andreasen Klahn, H. Cao, L. Spillecke, C. Koo, S. Spachmann, R. Klingeler, G. Rajaraman, J. Overgaard and M. Shanmugam, *Cell Reports Physical Science*, 2021, **2**, 100404.
3. L. J. Farrugia and C. Evans, *J Phys Chem A*, 2005, **109**, 8834-8848.
4. F. Cortes-Guzman, R. M. Gomez, T. Rocha-Rinza, M. A. Sanchez-Obregon and J. M. Guevara-Vela, *J Phys Chem A*, 2011, **115**, 12924-12932.
5. F. Neese, *WIREs Computational Molecular Science*, 2018, **8**, e1327.
6. T. A. Keith, AIMAll (19.10.12), TK Gristmill Software, Overland Park KS, USA, 2019.